Overview of results from the MST reversed field pinch experiment

Overview of results from the MST reversed field pinch experiment

J.S. Sarff[1], A.F. Almagri[1], J.K. Anderson[1], M. Borchardt[1], W. Cappechi[1], D. Carmody[1], K. Caspary[1], B.E. Chapman[1], D.J. Den Hartog[1], J. Duff[1], S. Eilerman[1], A. Falkowski[1], C.B. Forest[1], M. Galante[1], J.A. Goetz[1], D.J. Holly[1], J. Koliner[1], S. Kumar[1], J.D. Lee[1], D. Liu[1], K.J. McCollam[1], M. McGarry[1], V.V. Mirnov[1], L. Morton[1], S. Munaretto[1], M.D. Nornberg[1], P.D. Nonn[1], S.P. Oliva[1], E. Parke[1], M.J. Pueschel[1], J.A. Reusch[1], J. Sauppe[1], A. Seltzman[1], C.R. Sovinec[1], D. Stone[1], D. Theucks[1], M. Thomas[1], J. Triana[1], P.W. Terry[1], J. Waksman[1], G.C. Whelan[1], D.L. Brower[2], W.X. Ding[2], L. Lin[2], D.R. Demers[3], P. Fimognari[3], J. Titus[4], F. Auriemma[5], S. Cappello[5], P. Franz[5], P. Innocente[5], R. Lorenzini[5], E. Martines[5], B. Momo[5], P. Piovesan[5], M. Puiatti[5], M. Spolaore[5], D. Terranova[5], P. Zanca[5], V.I. Davydenko[6], P. Deichuli[6], A.A. Ivanov[6], S. Polosatkin[6], N.V. Stupishin[6], D. Spong[7], D. Craig[8], H. Stephens[9], R.W. Harvey[10], M. Cianciosa[11], J.D. Hanson[11], B.N. Breizman[12], M. Li[12] and L.J. Zheng[12]

[1] University of Wisconsin, and the Center for Magnetic Self-Organization in Laboratory and Astrophysical Plasmas, Madison, WI, USA
[2] The University of California at Los Angeles, Los Angeles, CA, USA
[3] Xantho Technologies, LLC, Madison, WI, USA
[4] Florida A&M University, Tallahassee, FL, USA
[5] Consorzio RFX, Associazione EURATOM-ENEA sulla Fusione, Padova, Italy
[6] Budker Institute of Nuclear Physics, Novosibirsk, Russia
[7] The Oak Ridge National Laboratory, Oak Ridge, TN, USA
[8] Wheaton College, Wheaton, IL, USA
[9] Pierce College, Lakewood, WA, USA
[10] CompX, Del Mar, CA, USA
[11] Auburn University, Auburn, AL, USA
[12] University of Texas at Austin, Austin, TX, USA

E-mail: jssarff@wisc.edu

Abstract

An overview of recent results from the MST reversed field pinch programme is presented. With neutral beam injection, bursty energetic particle (EP) modes are observed. The profiles of the magnetic and density fluctuations associated with these EP modes are measured using a far infrared interferometer–polarimeter. Equilibrium reconstructions of the quasi-single-helicity 3D helical state are provided by the V3FIT code that now incorporates several of MST's advanced diagnostics. The orientation of the helical structure is controlled using a new resonant magnetic perturbation technique. Gyrokinetic simulations based on experimental equilibria predict unstable trapped-electron modes (TEMs), and small-scale density fluctuations are detected in improved-confinement plasmas with TEM-like features. Upgraded pellet injection permits study of density and beta limits over MST's full range of operation, and an MST-record line-average density of 0.9×10^{20} m^3 ($n/n_G = 1.4$) has been obtained. Impurity ion temperature measurements reveal a charge-to-mass-ratio dependence in the rapid heating that occurs during a sawtooth crash. Runaway of NBI-born fast ions during the impulsive sawtooth event agrees with test-particle theory. Magnetic self-organization studies include measurements of the dynamo emf with an applied ac inductive electric field using oscillating field current drive.

Keywords: reversed field pinch, stellarator, energetic particles, gyrokinetics, density limit, beta limit

(Some figures may appear in colour only in the online journal)

1. Introduction

This overview of recent results from the MST reversed field pinch (RFP) programme summarizes physics important for the advancement of the RFP as well as for improved understanding of toroidal magnetic confinement in general. Topics discussed below are energetic particle (EP) effects, 3D helical equilibria, microturbulence, beta and density limit studies, ion heating, and magnetic self-organization physics. The MST is a large RFP experiment ($R = 1.5$ m, $a = 0.5$ m) that operates at medium plasma current ($I_p < 0.6$ MA) [1]. The world's other RFP experiments are RFX-mod in Italy, Extrap-T2R in Sweden, and RELAX in Japan. A new RFP experiment called KTX is under construction at the University of Science and Technology, Hefei, China, and is anticipated to begin operation in 2015 [2]. The RFP magnetic configuration offers several potential advantages for fusion. The RFP is not constrained by the Kruskal–Shafranov limit, and $q = aB_T/RB_p \ll 1$. Its relatively large plasma current allows the possibility for ohmic heating to burning plasma conditions. Large plasma current density also implies a large absolute magnitude for the empirical density limit, $n_G \sim I_p/\pi a^2$. Unlike configurations with large toroidal field, the magnetic field strength in the RFP is minimum at the magnets, allowing the possibility for normal conductors. These features promote a fusion power vision for high power density and high reliability through the use of relatively simple technology. In a more general fusion development context, the RFP's large magnetic shear and weaker toroidal effects complement the physics regimes of tokamak and stellarator plasmas. Hence RFP research helps advance the predictive capability of fusion plasma science by exploring parameter ranges that would otherwise be inaccessible.

2. EP modes and fast ion transport

A 1 MW neutral beam injector installed on MST allows investigation of energetic ion confinement and stability in the RFP [3]. This is unique capability within RFP research, and provides an important new experimental platform to validate critical EP physics. The neutral beam injection (NBI) source on MST is versatile in operating with a variable mixture of hydrogen and deuterium, and over a range of energies to its maximum of 25 keV. Previous work has shown that the NBI-generated fast ions have near-classical confinement, even when magnetic stochasticity dominates thermal transport [4]. This good confinement and strong beam focusing allows accumulation of a large fast ion population concentrated in the core of the plasma.

Several bursty $m = 1$ EP modes are observed that are consistent with continuum modes destabilized by the centrally peaked energetic ion density profile [3, 5–7]. The modes exhibit strong nonlinear coupling and are associated with fast ion loss or redistribution, as shown in figure 1. These data are based on a large ensemble of similar bursts; time is measured relative to the peak amplitude of the $n = 5$ EP mode, defined as $t = 0$. The magnetic spectrum of toroidal modes, $n < 32$, is measured by an array of 64 poloidal field pickup loops mounted on the inner surface of vacuum vessel, close to the surface of the plasma. The
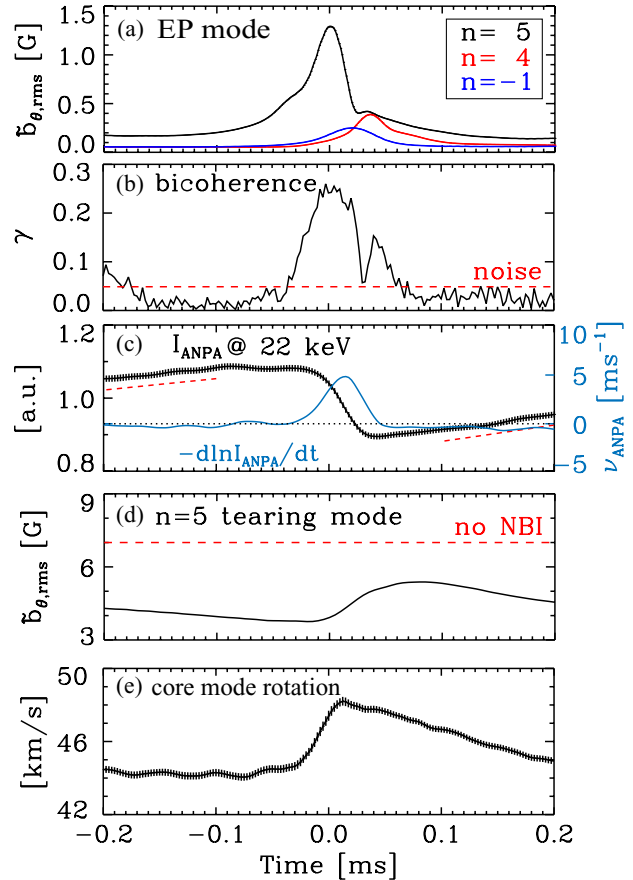
Figure 1. (*a*) EP-driven magnetic activity, (*b*) bicoherence, (*c*) core fast H content at a burst of the (5,4,−1) triplet; core tearing mode (*d*) amplitude and (*e*) rotation.

amplitudes of the EP modes are shown in figure 1(*a*). They have frequencies $f \sim 50$–200 kHz that depend on the plasma density, magnetic field strength, and ion mass [5] and only appear with NBI. Fast ion loss/redistribution is evidenced by a decrease in the high-energy neutral flux measured by an advanced neutral particle analyser (ANPA) [8], illustrated by the $\sim$22 keV energy channel in figure 1(*c*). The increase in the fast ion loss rate, $\propto -\text{d} \ln I_{\text{ANPA}}/\text{d}t$, corresponds with the appearance of modes $n = 4$ and $n = -1$. The three modes are strongly nonlinearly coupled, measured by the bicoherence in figure 1(*b*). Suppression of tearing instability with NBI is evidenced by a reduction in the amplitude of the core-resonant $n = 5$ tearing mode shown in figure 1(*d*), also measured by the pickup loop array. This mode rotates in the laboratory frame but its signal frequency ($f \lesssim 30$ kHz) is small compared to the EP mode frequency, which is easily separated by bandpass filtering and wavelet analysis [5, 6]. While there are many $m = 1$ tearing mode resonances across the plasma minor radius, the $n = 5$ mode is resonant closest to the magnetic axis where the fast ion density is concentrated. Its dynamics are therefore a secondary indicator of the fast ion density, and the sudden *increase* in the mode amplitude and rotation velocity in figures 1(*d* and *e*) are consistent with a loss or redistribution of the fast ion population.

The profiles of density fluctuations and, for the first time in a toroidal device, magnetic fluctuations associated with EP modes are measured using multi-chord far infrared (FIR)
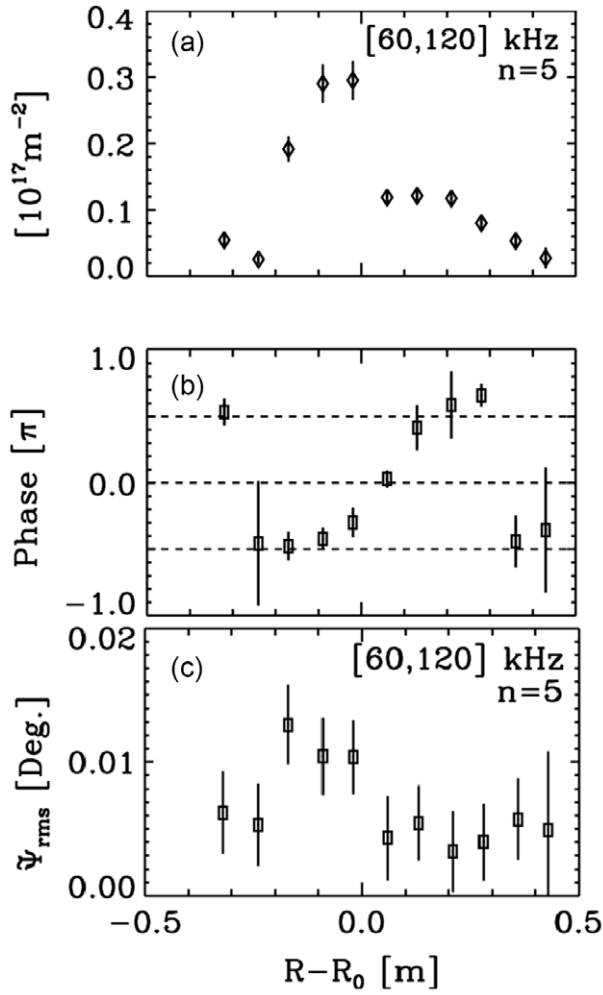
Figure 2. Profile of (*a*) rms amplitude, (*b*) relative phase of line-integrated density fluctuations, and (*c*) rms amplitude of fluctuations in the Faraday rotation measure for the $n = 5$ EPM. The amplitudes are obtained by bandpass filtering from 60–120 kHz, the range of frequency for the $n = 5$ mode, and averaging over the burst period $-0.1 < t < 0.1$ ms.

interferometry and polarimetry (Faraday rotation) [6]. The fluctuation amplitude profiles for the $n = 5$ EPM are peaked in the core, as shown in figure 2. The relative phase of the density fluctuation (figure 2(*b*)) suggests the character of the mode is compressional in the core and advective in the edge where the equilibrium density gradient is largest. The magnetic fluctuation is associated with the Faraday rotation measure $\tilde{\Psi} = c_{\mathrm{F}} \int (n_{\mathrm{e}0}\tilde{b}_z + \tilde{n}_{\mathrm{e}}B_{0z})\,\mathrm{d}z$, shown in figure 2(*c*). The portion due to the magnetic fluctuation is dominant and can be isolated by removing the contribution associated with the density fluctuation, yielding $\tilde{b}_z \approx \tilde{b}_r \approx 2\,\mathrm{G}$ in the core. The normalized amplitude is $\tilde{b}_r/B_0 \approx 7 \times 10^{-4}$. Measurement of the local magnetic fluctuation helps confirm the compressional nature of the EPM in the core, since a much larger $\tilde{b}_r \sim 14\,\mathrm{G}$ would be required for an advective response [6]. Looking forward, the capability to resolve both density and magnetic field structure will be extremely valuable to help understand the origin of these modes and their saturation and damping.
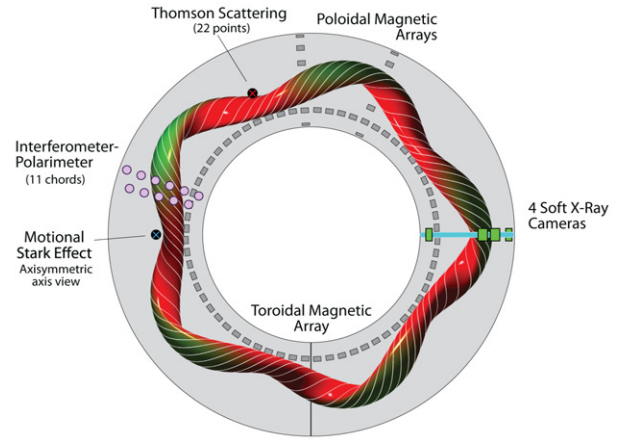
Figure 3. MST diagnostic coverage used for V3FIT 3D equilibrium reconstructions. A typical flux surface in the core region is shown for reference.

3. Controlling 3D equilibria in the QSH regime

The RFP plasma is subject to tearing instability driven by peaking of the parallel current profile, i.e. $\nabla(J_{\parallel}/B)$. While typically only a few modes resonant in the core are linearly unstable, the tearing spectrum is broad due to nonlinear mode–mode coupling processes. The mode amplitudes are then similar in magnitude, referred to as the multi-helicity regime. At high current the plasma spontaneously transitions towards a 3D helical equilibrium, called the quasi-single-helicity (QSH) regime [9], in which the innermost tearing mode grows to large amplitude while other modes in the spectrum are reduced in amplitude. The magnitude of the helical 3D magnetic field can approach that of stellarator configurations, particularly in the single-helical-axis (SHAx) limit where there is only one, helical magnetic axis. Recently it was shown that the onset of the QSH transition in MST and RFX-mod plasmas occurs for a similar value of the Lundquist number, $S = \tau_{\mathrm{R}}/\tau_{\mathrm{A}} \sim I_{\mathrm{p}}T_{\mathrm{e}}^{3/2}/\sqrt{n}$ [10]. In addition to the requirement for high plasma current, the QSH regime is most reliably attained in MST with $q(a) = 0$. This suggests the onset of QSH may be aided by removing the $q = 0$ magnetic surface from the plasma, thus interrupting nonlinear energy transfer associated with $m = 0$ tearing modes. The dominant mode in MST is $m = 1$, $n = 5$, consistent with the value of the safety factor $q(r = 0) \approx 1/5$.

Equilibrium reconstructions in the SHAx regime are performed using the V3FIT code [11], which is based on the VMEC equilibrium solver used extensively in stellarator research. Several of MST's advanced diagnostics are now incorporated in V3FIT, including FIR interferometry and polarimetry (Faraday rotation), as well as soft x-ray tomography. Available diagnostics and a representative V3FIT equilibrium reconstruction are shown in figure 3.

A new resonant magnetic perturbation (RMP) technique has been developed for controlling the orientation (mode phase) of the 3D structure [12]. The intrinsic rotation of QSH plasmas in MST typically slows as a consequence of magnetic braking [13], which is enhanced by the large amplitude of the dominant mode. The plasma locks to the wall with a mode phase that varies shot-to-shot but not quite randomly, shown as the green histogram in figure 4. MST's 5 cm-thick
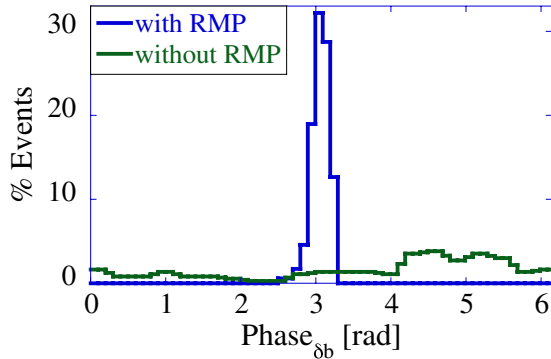
Figure 4. Distributions of the phase for the (locked) $n = 5$ mode with and without application of a resonant magnetic perturbation at the vertical shell cut. Each event corresponds to a separate discharge.
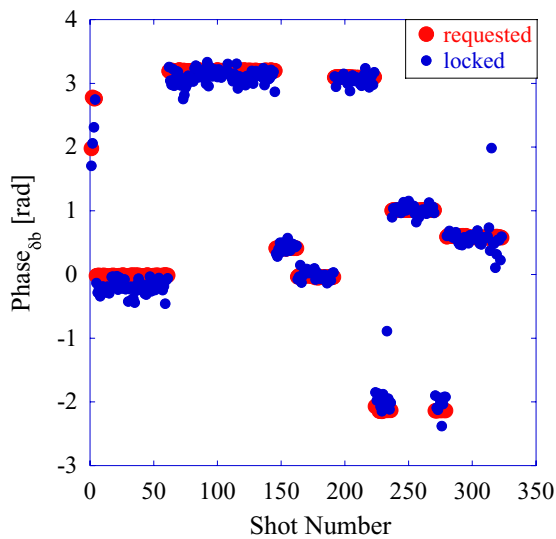
Figure 5. The locked phase is robustly adjustable and corresponds well to the requested phase, determined in advance by varying the phase of the RMP.

aluminum vacuum vessel has a vertical cut to allow magnetic field penetration, and a set of saddle coils placed over this cut are used to reduce the local magnetic field error associated with image current on the shell's inner surface. This system is feedback-controlled based on local measurements of the radial magnetic field at the cut. To control the locked phase of the 3D equilibrium, an $m = 1$ offset with a prescribed phase is imposed by the saddle coils. The toroidal mode spectrum of the applied field is broad (i.e. the cut has narrow width), but a portion of the magnetic perturbation is resonant in the plasma, allowing a phase-locked braking torque to be applied. This application of a localized magnetic field perturbation allows the phase to be controlled systematically, as shown by the blue histogram in figure 4 for one particular phase. The method is variable and robust, and the attained locked phase coincides well with the predetermined or 'requested' locked phase, as shown in figure 5. This has proven very useful for optimizing measurements of the 3D structure and related physics using MST's advanced diagnostics shown in figure 3 that do not all span the full minor diameter of the plasma.

The onset of the QSH regime has been studied extensively in nonlinear visco-resistive magnetohydrodynamics (MHD).

Indeed, a bifurcation from the nominally axisymmetric state to the helical state was observed computationally [14] prior to measurements of a robust 3D state in RFP experiments. Nevertheless the QSH transition is not completely understood. For example, experimentally the QSH transition tends to favour highest temperature conditions for which resistive dissipation is reduced. As discussed in [14], the Hartmann number, $H = S/P^{1/2}$, has been shown to parametrize the threshold for the transition to QSH in nonlinear MHD computation, where $S \sim \eta^{-1}$ is the Lundquist number and $P = \nu/\eta$ is the magnetic Prandtl number. While the experimental resistivity, η, is consistent with its classical value, less is known about the viscosity, ν, which has highly anisotropic classical values. Experimentally, ν appears to be anomalous [15, 16], and it is therefore likely reduced as well, since the QSH regime is accompanied by reduced magnetic fluctuations (either dynamically or through S-scaling).

A new and distinct theoretical model has been developed with predator–prey dynamics that capture key features of the QSH transition [17, 18]. This model invokes shear stabilization (either flow or magnetic) associated with 3D structure of the dominant mode to interrupt nonlinear mode–mode coupling that occurs in the multi-helicity regime. Experiments are planned using MST's diagnostic neutral beam for localized measurements of the flow, including its 3D structure. The DNB is currently being refurbished, but forward modelling is underway using V3FIT to evaluate diagnostic sensitivity to localized shear layers.

4. Microturbulence in the RFP

While stochastic magnetic transport dominates in the multi-helicity regime due to the presence of many tearing modes, confinement is enhanced ten-fold using pulsed inductive current profile control (PPCD) to mitigate tearing instability [19]. An internal transport barrier has also been identified in QSH plasmas [20]. In these improved-confinement regimes, transport in the RFP might ultimately be limited by drift-wave-like turbulence, as in tokamak and stellarator plasmas. Gyrokinetic simulations (GYRO and GENE) based on experimental toroidal equilibrium reconstructions of PPCD plasmas in MST predict unstable density-gradient-driven trapped-electron modes (TEMs) [21]. These simulations predict that the critical gradient is larger than for a typical tokamak plasma by roughly the aspect ratio, R/a, consistent with the relative difference in magnetic field scale length. Nonlinear simulations show that the 'Dimit's shift' due to strong zonal flows is relatively large, which persists even at finite beta, as shown in figure 6 [22].

Experimentally, coherent short wavelength density fluctuations have been detected by FIR forward scattering in PPCD improved-confinement plasmas. The pressure gradient is increased significantly in these plasmas, making them good candidates to observe drift wave instability. A frequency power spectrum is shown in figure 7 for an illustrative 0.4 MA plasma. The broadband decrease in fluctuation amplitude in the improved-confinement (PPCD) case is associated with the dramatic reduction in tearing instability with current profile control, revealing a new peak at $f \sim 100$ kHz. The fluctuations at this new peak have $k_\phi \rho_s \sim 0.2$, propagate in
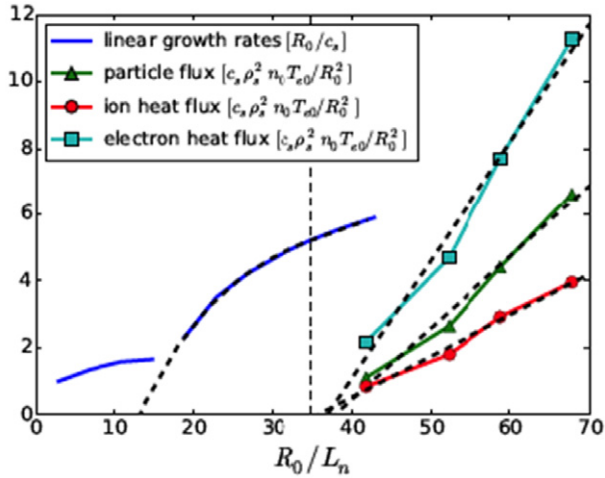
Figure 6. Predicted growth rate, heat fluxes, and particle flux of TEM turbulence versus the density gradient in modelling of 0.5 MA improved-confinement (PPCD) plasmas in MST.
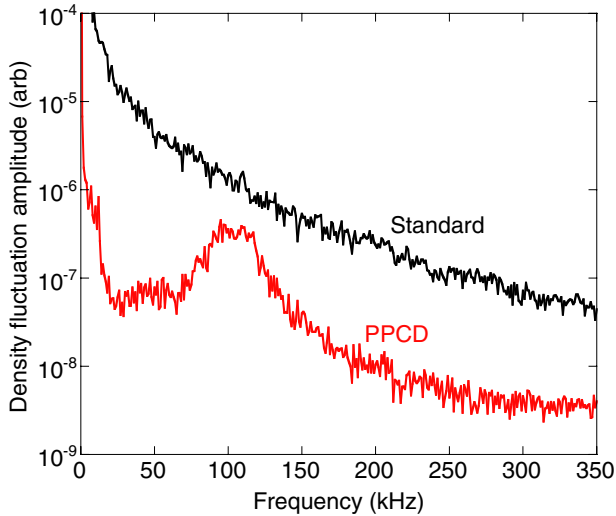
Figure 7. Density fluctuation at $r/a \approx 0.8$ measured by FIR forward scattering for 0.4 MA standard and improved-confinement plasmas (PPCD).

Figure 8. Density versus n_G for a wide range of MST plasmas with $I_p \leqslant 0.5$ MA. Highest density plasmas are attained with edge fuelling provided by pellet impact on the far wall.

the electron diamagnetic drift direction, and are localized to a region $r/a \sim 0.8$ where the equilibrium density gradient is maximum. The fluctuation amplitude also correlates with the experimental gradient scale length, exhibiting a threshold onset at $R/L_n \approx 35$. The electron temperature gradient is substantially increased as well, although deeper in the core. A weak correlation with ∇T_e is seen for these new fluctuations, but the T_e measurements in the edge region are currently not very precise and are being improved.

5. Limits to density and beta in MST plasmas

The RFP plasma exhibits a density limit that is qualitatively similar to the empirical limit, $n_G \propto I_p/\pi a^2$, observed in tokamak plasmas [23]. A recently completed upgrade to the frozen-gas pellet injector on MST has permitted a characterization of the density limit over MST's full range of plasma current $I_p \leqslant 0.5$ MA [24]. For this study the pellet parameters were chosen such that ablation within the plasma

was minimal, and the pellet's impact on the far wall provided a precisely controlled amount of edge fuelling with reduced impact on shot-to-shot variations in wall recycling. As the density approaches $n/n_G \rightarrow 1$, the plasma current begins to decrease, and for large enough density, the current terminates. This is phenomenologically similar to previous experiments using valve-controlled gas puffing. The attained density limit versus n_G is plotted in figure 8 for normal RFP plasmas with $q(a) < 0$ and for non-reversed plasmas with $q(a) = 0$. For all of these data, the transient $-I_p^{-1} dI_p/dt < 5\%$-ms. It is not clear why $q(a) = 0$ plasmas appear to have a modestly larger density limit.

Beta limit studies were performed in PPCD improved-confinement plasmas with the pellet parameters optimized for core ablation to maximize beta, with results similar to previously published work [25]. In this case, the density can well exceed n_G without premature termination, and an MST-record line-average density of 0.9×10^{20} m^3 ($n/n_G = 1.4$) has been obtained for 0.5 MA. Beta appears to saturate over a wide range of density, $0.2 < n/n_G < 1.6$, shown in figure 9. For most of these data a rough estimation of the electron beta is used to expose the trend over a wide range of plasma conditions for which full diagnosis was not available. Precise measurements of the total beta, $\beta = 2\mu_0 \langle p \rangle / B^2(a)$ were performed for a subset of the plasmas, with the values indicated by the blue coloured circles in figure 9. When pellet injection is combined with NBI, asymmetric ablation by the fast ion population produces a rocketing effect in the toroidal direction, aiding the localization of fuelling in the core.

6. Ion heating and energization

The ions in MST are typically much hotter than allowed by collisional relaxation with the inductively heated electrons.
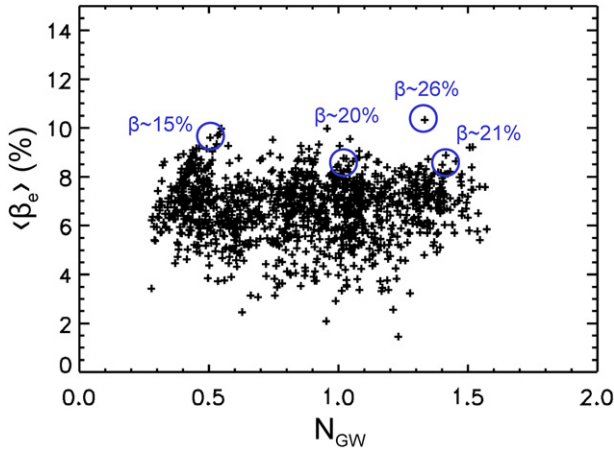
Figure 9. Electron $\beta_e = 2\mu_0 \overline{n}_e \overline{T}_e / B^2(a)$ versus normalized density for pellet-fuelled improved-confinement plasmas. Line-averaged values for n_e and T_e are used to expose the trend versus density, owing to diagnostic challenges at high density.
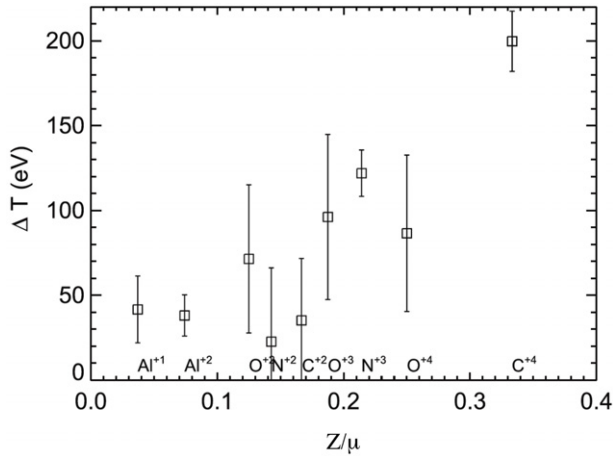
Figure 10. Increase in the temperature of various impurity ion species versus their charge-to-mass ratio.

The heating process is connected to tearing mode magnetic reconnection, but the detailed mechanism(s) is not yet understood. Previous measurements showed that the increase in majority ion temperature depends on the ion mass [26], impurity ions are hotter than the majority ions and heated anisotropically, with the perpendicular-to-**B** temperature ($T_\perp$) higher than the parallel-to-**B** temperature ($T_\parallel$) [27], and an energetic ion tail forms spontaneously [27]. New impurity ion temperature measurements using fast Doppler spectroscopy for several charge states of C, N, O and Al reveal a charge-to-mass-ratio dependence in the rapid heating, as shown in figure 10 [28]. These line-of-sight measurements are in the edge of the plasma and therefore reflect $T_\parallel$, but they are consistent with a dominantly perpendicular heating mechanism with collisional relaxation. A likely mechanism consistent with many of the measurements is gyro-resonant heating, proposed for both RFP [29] and the solar corona and wind plasmas [30].

The acceleration of energetic ions has also been measured [31, 32] and agrees very well with classical runaway expectations [33]. While electron runaway is well studied, there have been relatively few measurements of ion runaway,
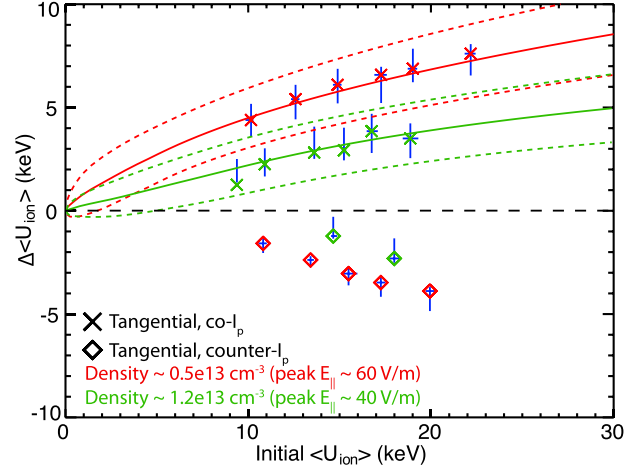
Figure 11. Energy gain of NBI-born fast ions during impulsive reconnection events. The (∗) data points are the measured post-event energy gain of fast ions for two plasma densities. Test-particle predictions for the energy gain due to runaway are shown by the solid curves, with uncertainty bounded by the dashed curves. Deceleration of the fast ions is observed with counter-current operation, shown by the (◇) data points.

e.g. ion heating in MAST plasmas [34]. In MST the equilibrium magnetic field changes abruptly during the sawtooth crash, which creates a large inductive electric field $E_\parallel \lesssim 50\,\mathrm{V\,m^{-1}}$. Energetic ions created by NBI are observed to increase in energy during these impulsive events, as shown in figure 11. The change in energy of the ions is measured by a neutral particle analyser that is most sensitive to low-pitch ions in the core. The initial energy of the ions is varied by adjusting the NBI voltage. The data agree well with the classical test ion expectations [33] as well as Fokker–Planck analysis. The direction of the inductive $E_\parallel$ can be controlled by changing the direction of the plasma current, which then decelerates the ions instead, also shown in figure 11. Despite their much higher mobility, a large runaway electron population is not observed, primarily a consequence of their relatively poor confinement in the stochastic magnetic field associated with the tearing modes [35]. (These measurements are in normal multi-helicity RFP plasmas.) In stark contrast, energetic ions have near-classical confinement, even in the stochastic field, as a result of their larger drifts [4]. While the measurements and analysis are for energetic ions, the good agreement with the fundamental theory underlying the runaway process supports the concern for electron runaway in ITER disruptions.

7. OFCD and magnetic self-organization

Oscillating field current drive (OFCD) is an inductive current drive method that could sustain the plasma current in steady state without long-term accumulation of magnetizing flux [36]. Sinusoidal applied toroidal and poloidal loop voltages are phased such that time-average dc magnetic helicity is injected into the plasma. Previous experiments on MST demonstrated 10% current drive by OFCD (figure 12), with little impact on energy confinement [37].

Just as for standard RFP operation, magnetic self-organization is active with OFCD such that the parallel current density tends towards a profile that is marginally unstable to
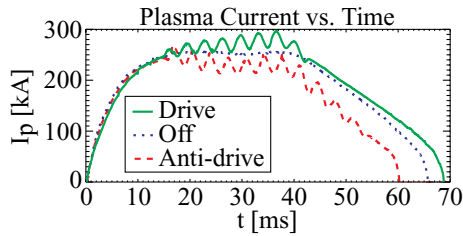
Figure 12. Partial current drive with OFCD in MST. The drive and anti-drive cases are obtained by controlling the relative phase of the loop voltage oscillations to increase and decrease magnetic helicity injection, respectively [38].
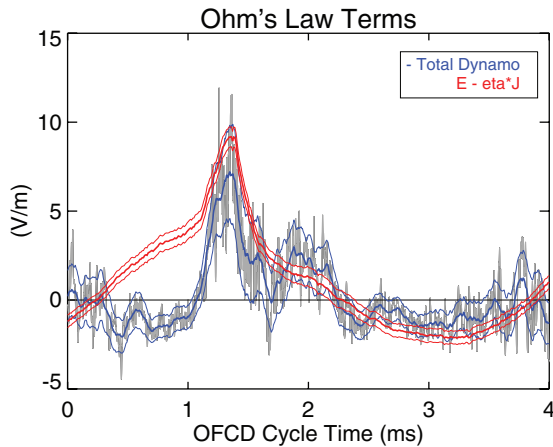
Figure 13. Measurement of terms in parallel Ohm's law during an OFCD cycle.

tearing modes [39]. However, for part of the OFCD oscillation cycle, the applied inductive electric field supports the current in the outer region of the plasma where it is normally sustained by a dynamo-like emf, $\langle \tilde{V}_e \times \tilde{B} \rangle_{||} = \langle \tilde{E} \cdot \tilde{B} \rangle / \langle B \rangle$, associated with the tearing fluctuations. A novel capacitive probe was used to measure $\tilde{E}$ and thereby the emf at a location in the edge region of plasma, time-resolved over an OFCD cycle, as shown in figure 13 [40]. Magnetic pickup loops are included in the probe to measure the local $\tilde{B}$. This is similar to earlier measurements on MST [41]. Since Ohm's law stems from electron force balance, $\langle \tilde{V}_e \times \tilde{B} \rangle_{||}$ represents the complete dynamo emf even if two-fluid effects are important, as implied by previous measurements of the Hall term, $\langle \tilde{J} \times \tilde{B} \rangle_{||} / en_e$ in MST plasmas [42, 43], and recent two-fluid NIMROD computations [44]. The near-balance of parallel Ohm's law, $E_{||} + \langle \tilde{V}_e \times \tilde{B} \rangle_{||} = \eta J_{||}$ further supports the OFCD physics basis. Unfortunately, due to the concomitant oscillation of the equilibrium field, a larger and hotter plasma is required to demonstrate full current sustainment by OFCD [39].

8. Summary

Rapid progress continues to be made investigating energetic ion confinement and stability in the RFP using a high power neutral beam injector (NBI) installed on MST. Instabilities associated with NBI are observed for the first time in the RFP, with features of energetic-particle-type modes that exhibit nonlinear interaction and affect fast ion transport. Modelling

of these instabilities has begun using several theoretical approaches.

Progress in understanding and controlling the 3D helical equilibrium in the quasi-single helicity (QSH) regime has been enhanced by the development of equilibrium reconstructions using the V3FIT code together with MST's advanced diagnostic set. This is a good example of RFP research that helps advance analysis tools that are important in all magnetic configurations. A resonant magnetic perturbation method has been developed to control the locked phase of the helical structure. A new predator–prey theoretical model introduces a distinct path towards theoretical understanding of the QSH transition.

An exciting new direction in RFP research is the possibility that microturbulence becomes important in improved-confinement regimes obtained when tearing instability is reduced. New short wavelength density fluctuations are measured in MST inductive-control plasmas using FIR far forward scattering. Modelling using the GENE code predicts unstable density-gradient-driven trapped-electron modes for these type of improved-confinement plasmas. This combination of experimental and theoretical research provides a valuable new arena to explore drift-wave-type instabilities that are important in magnetically confined plasmas generally.

An upgrade to the frozen pellet injector on MST has allowed investigation of the empirical density limit in MST plasmas over the full range of current operation. In standard confinement RFP plasmas, the limit is numerically similar to that observed for both RFP and tokamak plasmas, as seen in previous experiments. This limit can be exceeded in improved-confinement plasmas with core pellet fuelling. There is evidence for beta saturation in the improved-confinement case, a topic that will be further explored in the future.

The RFP plasma is well known for its magnetic self-organization behaviour. A particularly striking behaviour is ion heating that far exceeds collisional coupling to the ohmically heated electrons. New data shows that the ion heating at sawtooth magnetic reconnection events has a charge-to-mass ratio dependence, which provides an additional signature for this not yet well understood process. An elegant demonstration of the runaway of energetic ions has also been obtained by studying the inductive acceleration of NBI-generated fast ions. The measurements agree very well with test-particle theory for the runaway process. The self-organization associated with current profile relaxation has also been studied in plasmas with oscillating field current drive applied, and an observed balance in Ohm's law provides further experimental support for this intriguing steady-state current sustainment concept using an inductive electric field.

References

[1] Dexter R., Kerst D., Lovell T., Prager S. and Sprott J. 1991 *Fusion Technol.* **19** 131

[2] Liu W. *et al* 2014 *Plasma Phys. Control. Fusion* **56** 094009

[3] Anderson J.K. *et al* 2013 *Phys. Plasmas* **20** 056102

[4] Fiksel G. *et al* 2005 *Phys. Rev. Lett.* **95** 125001

[5] Koliner J.J. *et al* 2012 *Phys. Rev. Lett.* **109** 115003

[6] Lin L. *et al* 2013 *Phys. Plasmas* **20** 030701

[7] Lin L. *et al* 2014 *Phys. Plasmas* **21** 056104

[8] Eilerman S., Anderson J.K., Reusch J.A., Liu D. and Fiksel G. 2012 *Rev. Sci. Instrum.* **83** 10D302-1

[9] Lorenzini R. *et al* 2009 *Nature Phys.* **5** 570

[10] Sarff J. *et al* 2013 *Nucl. Fusion* **53** 104017

[11] Hanson J.D., Hirshman S.P., Knowlton S.F., Lao L.L., Lazarus E.A. and Shields J.M. 2009 *Nucl. Fusion* **49** 075031

[12] Munaretto S. *et al* 2015 Control of 3D equilibria with RMPs in MST *Plasma Phys. Control. Fusion* submitted

[13] Chapman B.E., Fitzpatrick R., Craig D., Martin P. and Spizzo G. 2004 *Phys. Plasmas* **11** 2156

[14] Cappello S. and Escande D.F. 2000 *Phys. Rev. Lett.* **85** 3638

[15] Almagri A.F., Chapman J.T., Chiang C.S., Craig D., Den Hartog D.J., Hegna C.C. and Prager S.C. 1998 *Phys. Plasmas* **5** 3982

[16] Terranova D., Bolzonella T., Cappello S., Innocente P., Marrelli L. and Pasqualotto R. 2000 *Plasma Phys. Control. Fusion* **42** 843

[17] Kim J.-H. and Terry P.W. 2012 *Phys. Plasmas* **19** 122304

[18] Terry P.W. and Whelan G.G. 2014 *Plasma Phys. Control. Fusion* **56** 094002

[19] Sarff J.S. *et al* 2003 *Plasma Phys. Control. Fusion* **45** A457

[20] Lorenzini R. *et al* 2012 *Nucl. Fusion* **52** 062004

[21] Carmody D., Pueschel M.J. and Terry P.W. 2013 *Phys. Plasmas* **20** 052110-1

[22] Carmody D., Pueschel M.J., Anderson J.K. and Terry P.W. 2015 *Phys. Plasmas* **22** 012504-1

[23] Greenwald M. 2002 *Plasma Phys. Control. Fusion* **44** R27

[24] Caspary K.J. 2014 Density and beta limits in the Madison symmetric torus reversed-field pinch *PhD Thesis* University of Wisconsin-Madison

[25] Wyman M. *et al* 2009 *Nucl. Fusion* **49** 015003

[26] Fiksel G., Almagri A.F., Chapman B.E., Mirnov V.V., Ren Y., Sarff J.S. and Terry P.W. 2009 *Phys. Rev. Lett.* **103** 145002

[27] Magee R.M., Hartog D.J.D., Kumar S.T.A., Almagri A.F., Chapman B.E., Fiksel G., Mirnov V.V., Mezonlin E.E. and Titus J.B. 2011 *Phys. Rev. Lett.* **107** 065005

[28] Kumar S.T.A., Almagri A.F., Craig D., Den Hartog D.J., Nornberg M.D., Sarff J.S. and Terry P.W. 2013 *Phys. Plasmas* **20** 056501-1

[29] Tangri V., Terry P.W. and Fiksel G. 2008 *Phys. Plasmas* **15** 112501

[30] Cranmer S., Field G. and Kohl J. 1999 *Astrophys. J.* **518** 937

[31] Eilerman S. 2014 Ion runaway during magnetic reconnection in the reversed-field pinch *PhD Thesis* University of Wisconsin-Madison

[32] Eilerman S., Anderson J.K., Sarff J.S., Forest C.B., Reusch J.A., Nornberg M.D. and Kim J. 2015 *Phys. Plasmas* **22** 020702-1

[33] Furth H.P. and Rutherford P.H. 1972 *Phys. Rev. Lett.* **28** 545

[34] Helander P., Eriksson L.-G., Akers R.J., Byrom C., Gimblett C.G. and Tournianski M.R. 2002 *Phys. Rev. Lett.* **89** 235002

[35] O'Connell R. *et al* 2003 *Phys. Rev. Lett.* **91** 045002

[36] Bevir M.K., Gimblett C.G. and Miller G. 1985 *Phys. Fluids* **28** 1826

[37] McCollam K.J. *et al* 2010 *Phys. Plasmas* **17** 082506

[38] McCollam K.J., Blair A.P., Prager S.C. and Sarff J.S. 2006 *Phys. Rev. Lett.* **96** 035003

[39] Ebrahimi F., Prager S.C., Sarff J.S. and Wright J.C. 2003 *Phys. Plasmas* **10** 999

[40] Stone D.R. 2013 Magnetic relaxation during oscillating field current drive in a reversed field pinch *PhD Thesis* University of Wisconsin-Madison

[41] Ji H., Almagri A.F., Prager S.C. and Sarff J.S. 1994 *Phys. Rev. Lett.* **73** 668

[42] Kuritsyn A., Fiksel G., Almagri A.F., Brower D.L., Ding W.X., Miller M.C., Mirnov V.V., Prager S.C. and Sarff J.S. 2009 *Phys. Plasmas* **16**

[43] Ding W.X., Brower D.L., Deng B.H., Almagri A.F., Craig D., Fiksel G., Mirnov V., Prager S.C., Sarff J.S. and Svidzinski V. 2006 *Phys. Plasmas* **13** 112306

[44] King J.R., Sovinec C.R. and Mirnov V.V. 2012 *Phys. Plasmas* **19** 055905